NANO LETTERS

Letter

Cite This: *Nano Lett.* 2018, 18, 3282−3289

pubs.acs.org/NanoLett

Activation of Human Natural Killer Cells by Graphene Oxide-Templated Antibody Nanoclusters

Christian Loftus,[†,‡,§] Mezida Saeed,[§] Daniel M. Davis,*[,§] and Iain E. Dunlop*[,‡]

[†]Department of Chemistry and [‡]Department of Materials, Imperial College London, Exhibition Road, London SW7 2AZ, United Kingdom

[§]Manchester Collaborative Center for Inflammation Research, University of Manchester, 46 Grafton Street, Manchester M13 9NT, United Kingdom

Supporting Information

ABSTRACT: An emerging new paradigm is that immune cell activation is controlled by transient interactions between supramolecular assemblies of receptors and ligands. Current immunotherapy biologic pharmaceuticals that activate or desensitize NK cells are, however, individual molecules that do not replicate this nanoscale organization of proteins. Here, we use nanoscale graphene oxide (NGO) as a template to generate soluble nanoscale clusters of Natural Killer cell-activating antibodies. We control nanocluster size and molecular number to mimic reported values for cell surface proteins. These NGO-templated molecular nanoclusters, used to stimulate NK cells via the CD16 receptor, successfully induced cellular activation, indicated by degranulation of cytolytic granules and IFN-γ secretion. Importantly, activation significantly exceeded that induced by the same antibodies applied as a solution of individual molecules. These results demonstrate that future immunotherapies could be enhanced by assembling immunomodulatory drugs into nanoclusters and establish NGO-templating as a candidate technology.

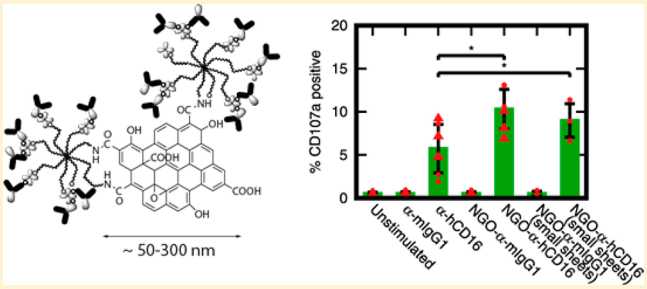

KEYWORDS: *Bionanotechnology, biofunctional nanoparticles, graphene oxide, NK cell, immune cell activation*

Immunotherapies are revolutionizing cancer treatments, as the focus shifts from drugs that kill tumors directly, toward harnessing the body's natural immune defenses.[1−3] Key players include leukocytes such as T cells[4,5] and closely related Natural Killer (NK) cells.[6,7] These recognize target cells and communicate with other immune cells via intimate cell−cell contacts, known as immunological synapses.[8−11] Importantly, the majority of interactions in immunological synapses are not between isolated ligand−receptor pairs but rather involve clusters of cell surface molecules in the size range 10−400 nm.[12−15] The size of these clusters correlates with cell signaling, and evidence is emerging that such nanostructural changes may be key drivers of immune cell activation.[13,15−19]

However, the importance of nanoscale clustering has not fed through into immunotherapy biologic agents for activating immune cells. Monoclonal antibodies, for example, each bind only a single Fc receptor such as the NK cell activating receptor CD16. This can impact on signaling, for example, Rituximab, one of the best-characterized antibodies used medically, activates NK cells when it is bound to a surface such as the surface of a target cell (in this case a B cell), but only weakly induces activation as an unbound soluble reagent.

Here, we have created an acellular soluble reagent that exploits receptor nanoclustering to activate immune cells. This consists of artificial clusters of leukocyte-stimulating ligands that mimic immunoreceptor nanoclusters in terms of size and molecular number. Specifically, the ligand molecules are mounted on a scaffold of functionalized nanoscale graphene oxide (NGO). NGO's planar shape means that they can extend to large (>50 nm) sizes without imposing the sharp curvatures associated with, for example, spherical nanoparticles, which would likely influence activation.[20] Furthermore, NGO is functionalizable and variants have been proposed for drug delivery, diagnostics, and phototherapy.[21−24]

We have demonstrated the efficacy of NGO-templated biomimetic nanoclusters as immune cell activating reagents in NK cells. Here, we focus on one of the best-characterized NK cell activating receptors, CD16, which recognizes the Fc portion of antibodies that have coated target cells, inducing target cell lysis (antibody-dependent cellular cytotoxicity, ADCC) and cytokine secretion.

We first developed a protocol to prepare antibody-functionalized NGO sheets of high purity and colloidal stability with direct knowledge of sheet size and molecular number. This has been applied to generate NGO functionalized with monoclonal antibodies that bind human CD16 with sheet size and molecular number in the correct range for cell surface receptor nanoclusters observed in super-resolution studies of leuko-

Received: March 18, 2018
Revised: April 12, 2018
Published: April 20, 2018

DOI: 10.1021/acs.nanolett.8b01089
Nano Lett. 2018, 18, 3282−3289

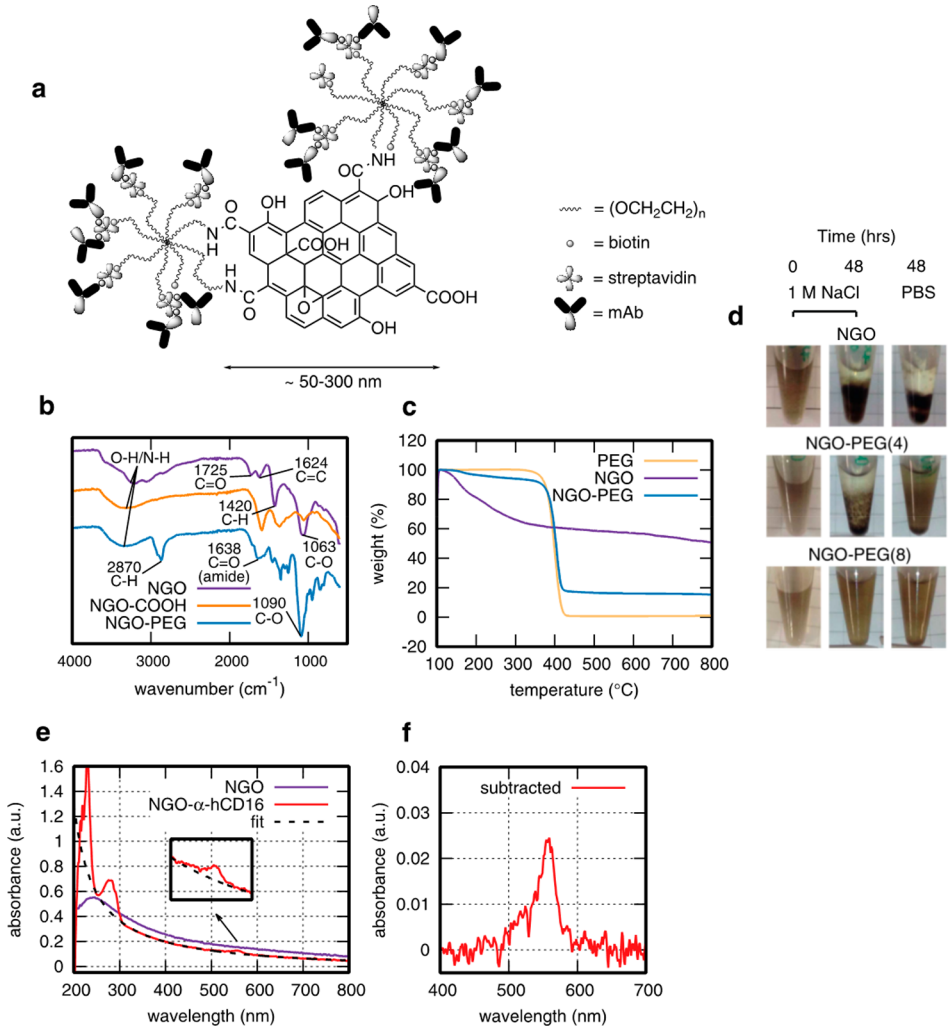

Figure 1. Characterization of NGO-templated antibody nanoclusters. (a) Schematic of NGO functionalization (not to scale). (b) IR spectra of GO, NGO−COOH, and NGO-PEG showing characteristic absorbances related to the successful conjugation of 8-arm star-PEG-NH_2 to NGO−COOH at 1638 cm^{-1} (amide C═O stretch) and 3870 cm^{-1} (ether C−H stretch), which are not observed in GO or NGO−COOH. (c) TGA profile of NGO-PEG, with reference profiles for PEG and NGO as separate species. (d) 8-arm PEGylation of NGO eliminates visible flocculation in 1 M NaCl and PBS in contrast to 4-arm PEGylation and as-received NGO. (e) UV−visible spectrum of NGO-mAb molecular nanoclusters with fluorescent dye-conjugated antibodies, showing protein and dye-associated peaks below 300 nm and dye-alone peak at 546 nm (expanded in inset). (f) Inset data with fit to NGO subtracted for UV−visible quantification of antibody functionalization.

cytes.[12,13,15,25,26] These artificial nanoclusters are confirmed to specifically bind primary human NK (pNK) cells via the CD16 receptor. Critically, they function as an activating reagent, enhancing NK cell effector functions in terms of both cytolytic responses as indicated by increased levels of cell-surface CD107a, a marker of degranulation, and the secretion of the cytokine IFN-γ.

Development of NGO-Templated Biomolecular Nanoclusters. A key property of biomolecular nanoclusters in the immune synapse is size, and our artificial nanoclusters should be synthesized in a realistic size range. Because super-resolution data on nanocluster sizes is only available for a few molecules, not currently including CD16, we chose to construct nanoclusters with a median size (diameter) of ~150 nm, similar to that observed for the NK cell surface receptor KIR2DL1[15] and in the middle of the reported range for TCR nanoclusters in activated T cells.[12] This was achieved using NGO flakes (2D-Tech, Manchester, U.K.) with purification steps carried out postfunctionalization delivering a narrow size distribution (see below).

A schematic of the chemical approach we developed to construct NGO-templated antibody nanoclusters is given in Figure 1a with nanocluster characterization shown in Figure 1b−g. Because our aim was to deliver a soluble stimulation system, and unfunctionalized NGO is unstable in salt concentrations of biological relevance, the first requirement was to functionalize the NGO with a stabilizing poly(ethylene glycol) (PEG) coating. PEG is widely used to protect bionanomaterials from flocculation and nonspecific interactions with proteins. PEGylated NGO specifically has been shown to be viable for in vivo applications with low toxicity and effective long-term clearance[27] as have other highly purified NGO materials.[28] Here, PEG-coating was achieved by first coupling carboxylic acid groups to the NGO surface and then binding amine-terminated PEG via EDC-activation of the carboxylic acid groups. Looking directly at colloidal stability, 8-arm star PEG (M_w 40 kDa, amine-terminated arms) was effective in stabilizing NGO at physiologically comparable salt concentrations, whereas 4-arm star-PEG (M_w 20 kDa) was not (Figure 1d), hence the 8-arm was used throughout. Successful

DOI: 10.1021/acs.nanolett.8b01089
Nano Lett. 2018, 18, 3282−3289

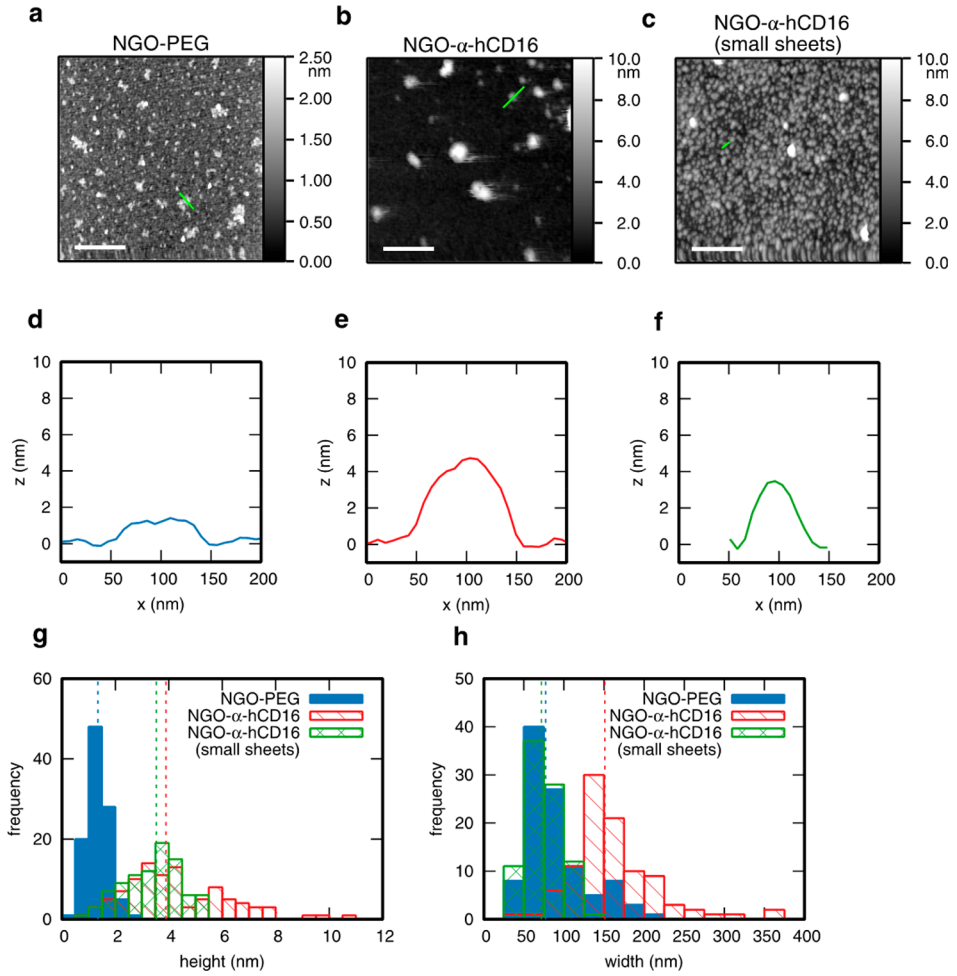

Figure 2. Individualized characterization of NGO-mAb nanoclusters by atomic force microscopy (AFM). (a) Representative AFM image of NGO-PEG sample deposited onto a silicon substrate (Tapping Mode measured in air). (b,c) Similar images of NGO-α-hCD16 molecular nanoclusters from two distinct size populations separated by a centrifugation protocol as described in the text. Scales bars all 500 nm. (d–f) Cross sections of typical nanosheets marked by green lines in images a–c. (g,h) Measured height and width distribution of NGO-PEG (101 objects measured), and the two separated NGO-α-hCD16 populations (98 sheets for the larger and 89 sheets for the smaller population). Dashed lines represent the median value for each histogram matched by color.

conjugation of PEG was confirmed by infrared (IR) spectroscopy with the appearance of C=O (amide, 1638 cm^{-1}) and ether C–H (3870 cm^{-1}) absorbances (Figure 1b). The quantity of attached PEG was determined using thermogravimetric analysis (TGA) (Figure 1c), giving 70 ± 5 wt % for a typical set of conditions.

To attach cell-stimulating molecules, we chose biotin–streptavidin linkage because this is highly flexible for the subsequent choice of attached biomolecules. Biotin groups were first linked to the remaining free amine groups on the star-PEG, at a sufficient density to saturate streptavidin adsorption on the NGO surface (~1 biotin per 11 nm^2). The resultant NGO-star-PEG-biotin was then streptavidin-coated, using streptavidin at a large excess to mimimize cross-linking between sheets,[29] purified by centrifugal filtration, and streptavidin conjugation was confirmed by UV–visible spectroscopy at 280 nm (Figure 1d). The streptavidin-coated NGO-PEG-biotin was then conjugated with antibody molecules that had been fluorescently labeled (AlexaFluor546, ~ 1 fluorophore per antibody molecule) and biotinylated at an optimal level to again mimimize intersheet cross-linking (~6 biotins per antibody molecule). This delivered the desired antibody-conjugated NGO nanoclusters with minimal free antibody as confirmed by centrifugation and UV–visible spectroscopy of the supernatant.

To apply controlled nanoscale stimulation to NK cells, we paid precise attention to quantifying the nanocluster size and the number of molecules per nanocluster, and to removing unconjugated biomolecules that might provide additional stimulation to cells. These requirements are in excess of previous studies where NGO-antibody conjugates produced by various methods are applied to drug delivery or diagnostic targeting.[21,22,30]

Accordingly, we have quantified the size distribution for each batch of antibody-NGO prepared by atomic force microscopy (AFM) (Figure 2a–h). In a typical example (Figure 2b,e), the lateral size of the antibody-NGO nanoclusters is 151 $\pm \frac{35}{24}$ (median value with ± indicating interquartile range) (Figure 2h), hitting the target size range outlined above. The height is 3.9 $\pm \frac{1.7}{1.0}$ nm (similarly indicated as the median with + and − indicating the locations of the first and third quartiles, similarly throughout this section) consistent with a single NGO sheet functionalized on both sides, and substantially greater than the height of NGO-PEG alone (Figure 2a,d). The number of antibody molecules per NGO-Ab nanocluster was determined by quantifying the concentrations of NGO and antibody using

DOI: 10.1021/acs.nanolett.8b01089
Nano Lett. 2018, 18, 3282–3289

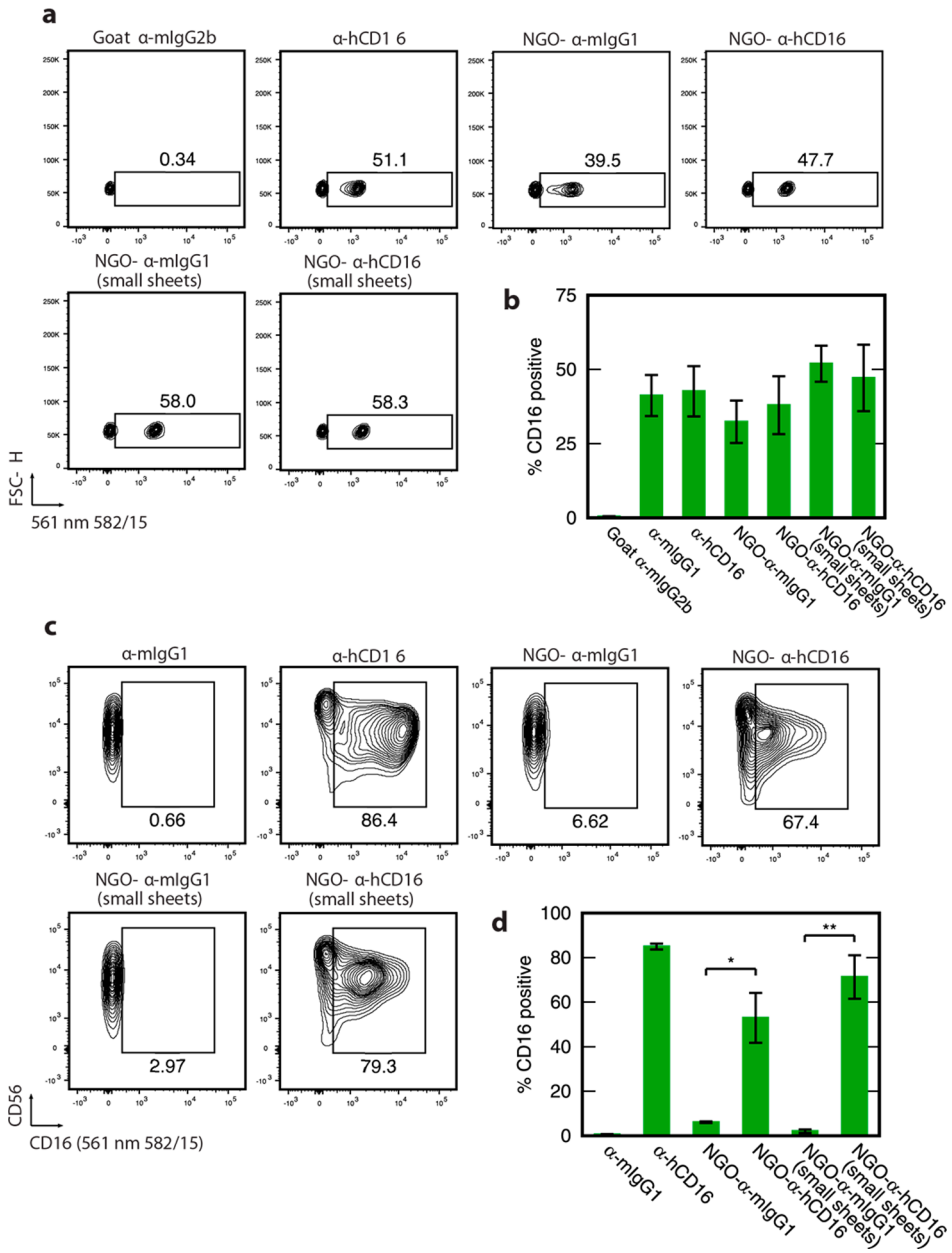

Figure 3. NGO-mAb molecular nanoclusters present antibody and NGO-α-hCD16 specifically binds pNK cells. (a) Flow cytometry for pNK cells incubated with a 1:1 mixture of polystyrene beads that are coated with α-mIgG1 and uncoated beads: 50% positive corresponds to maximum binding (within error). Typical results are shown for both NGO-α-mIgG1 and NGO-α-hCD16 nanoclusters. Negative and positive control experiments used soluble antibodies (α-mIgG2b and α-hCD16, respectively. (b) Quantification showing mean and standard deviation across two microbead samples. (c) Cell-binding. Flow cytometry data showing binding of pNK cells by nanographene oxide-templated nanoclusters NGO-α-hCD16 versus the negative control nanocluster NGO-α-mIgG1 and soluble antibody controls (α-mIgG1 and α-hCD16). The horizontal axis labeled either CD16 or (561 nm 582/15) refers to the fluorescence intensity detected at 563−591 nm and associated with the added antibody or nanocluster in each case. These are representative data using cells from a single donor. (d) Quantification of the binding to pNK cells of NGO-α-hCD16 nanoclusters and the other species used in panel c, showing mean and standard deviation of results from 3 human donors. Statistical significance is indicated as * $p < 0.05$, ** $p < 0.01$ (two-tailed paired parametric t-test). All contour plots are 5%, that is, 20 contour lines.

UV−vis spectroscopy (Figure 1e,f) and combining with the nanocluster size from AFM. For the 151 nm NGO-α-hCD16, there were 133 $\pm \frac{71}{39}$ antibody molecules per nanocluster or ~60−70 molecules per side, considering that only one side of the sheet-like nanocluster will bind the cell. This is in 2−3 fold excess of the, for example, 20−30 receptors per nanocluster reported for TCR nanoclusters, providing a physiologically plausible stimulus allowing for the fact that a fraction of the binding sites may be obstructed. Values of sheet lateral size and number of molecules were consistent within scatter across similarly prepared batches.

We found that the size of the NGO sheets could be controlled by varying the amount of postfunctionalization centrifugation, since larger nanoclusters pellet first. Batches of different sheet sizes were obtained by repeated centrifugation steps after antibody conjugation, removing the supernatant each time. Specifically, nanocluster lateral size was reduced from 151 $\pm \frac{35}{24}$ nm to 72 $\pm \frac{19}{11}$ nm by collecting the supernatant

DOI: 10.1021/acs.nanolett.8b01089
Nano Lett. 2018, 18, 3282−3289

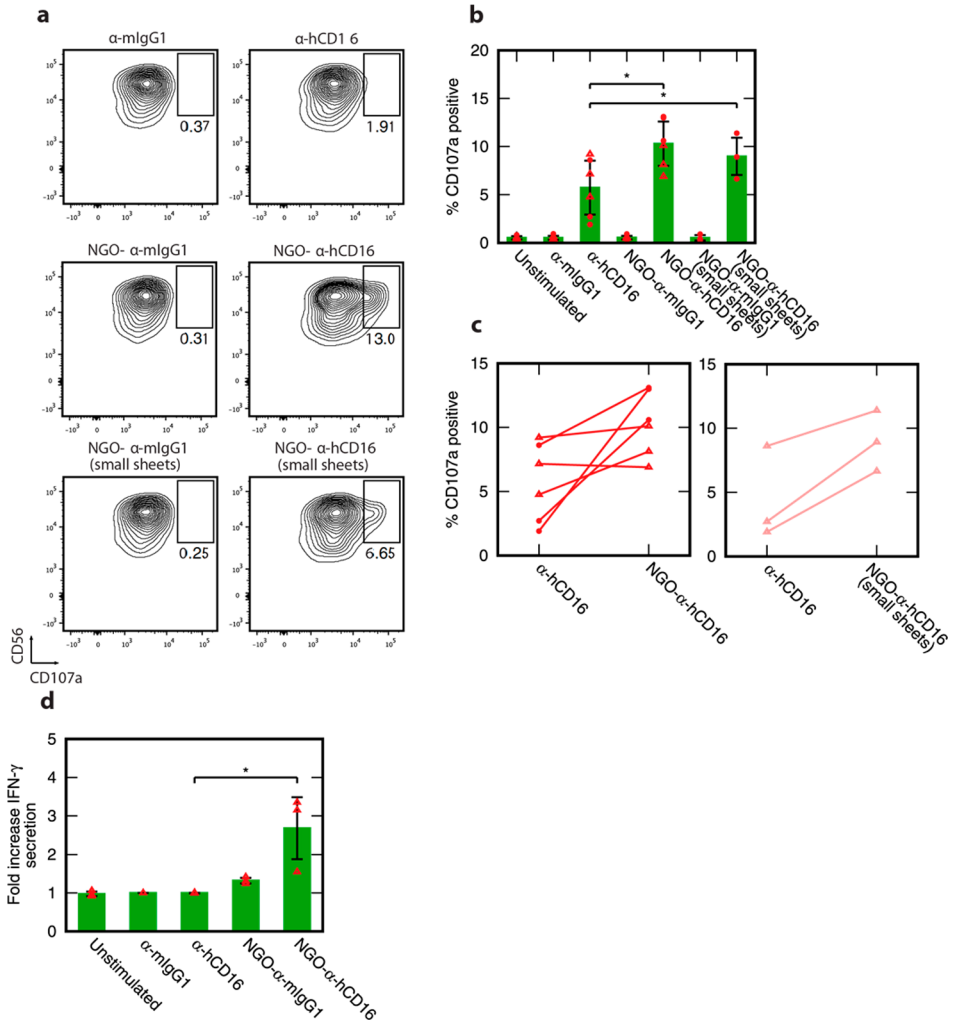

Figure 4. pNK cell activation is augmented through ligation using nanoclustered antibodies in the form of NGO-α-hCD16. (a) Representative flow cytometry plots of CD107a-stained pNK cells showing response to stimulation with NGO-templated antibody nanoclusters and control experiments with soluble antibodies. (b) Quantification of the percentage of CD107a positive cells as per part a, for both larger (~150 nm) and smaller (~70 nm) NGO-α-hCD16 nanoclusters: mean and standard deviation across three human donors for each NGO-α-hCD16 batch (and two separately prepared batches in the ~150 nm case). (c) Donor-by-donor comparison of CD107a expression in response to NGO-α-hCD16 and soluble antibody stimulation. Solid lines couple results from the same donor. (d) Average fold increase in IFN-γ secretion above the mouse IgG1 control for pNK cells stimulated with NGO-mAb nanoclusters (size ~150 nm) and with soluble α-hCD16: mean and standard deviation across three human donors. Statistical significance in panel b is indicated as * $p < 0.05$ (two-tailed paired parametric t-test), and panel d * $p < 0.05$ (two-tailed unpaired parametric t-test). All contour plots are 5%, that is, 20 contour lines.

after the third rather than the first centrifugation (small sheets in Figure 2C,f–h).

NGO-α-hCD16 Nanoclusters Present Antibody, Bind Specifically to Primary Human NK Cells (pNK cells). To confirm that NGO-anchored biomolecules were functionally accessible, we first determined their ability to bind commercial polystyrene beads that had been coated with antimouse IgGκ (α-mIgGκ) antibodies that recognize the antibodies on both NGO-α-hCD16 and the control NGO-α-mIgG1 nanoclusters. Readout was generated using flow cytometry and exploiting the AlexaFluor546 labeling of the NGO-conjugated antibodies. To facilitate direct comparison between antibody immobilized in nanoclusters and free individual antibody molecules, we used the same overall antibody concentration in both cases. A 1:1 mix of coated and uncoated beads was used. For both the NGO-mAb sheets, clear binding to the beads was shown (Figure 3a,b). Indeed, NGO-α-hCD16 nanoclusters bound ~100% of the coated beads (~50% overall). For NGO-α-mIgG1, the binding effectiveness was slightly lower at ~80% of coated beads (~40% overall).

The first requirement for NGO-α-hCD16 nanoclusters to perform their intended function of influencing NK cell activity is that they bind to NK cells via the CD16 receptor. We tested this using flow cytometry to analyze binding to pNK cells from peripheral blood, again using fluorescently labeled nanoclusters. To determine the extent that these cells expressed CD16, cells from each donor were tested using a solution of individual antibodies as well as the same antibody immobilized to nanoclusters. Again, an identical overall antibody concentration (2 μg/mL, sufficient to saturate all expressed receptors. Figure S1) was applied to cells in the two cases (soluble individualized antibodies and NGO-α-hCD16 nanoclusters).

Using this protocol, we showed that NGO-α-hCD16 nanoclusters bind effectively to pNK cells with an average of 53% of cells positively stained across three donors (Figure 3c,d) in the case of the 151 nm NGO-α-hCD16. This contrasts with

DOI: 10.1021/acs.nanolett.8b01089
Nano Lett. 2018, 18, 3282–3289

only 6% positive cells when the control NGO-α-mIgG1 nanoclusters are used ($p < 0.05$), demonstrating that the binding is mediated by the specificity of the α-hCD16 antibody. The same qualitative result is observed for the smaller 72 nm NGO-α-hCD16 nanoclusters. These results also demonstrate that our nanocluster synthesis protocol is effective in eliminating nonspecific binding to these cells. Kinetic measurements (Figure S2) showed slightly slower binding to pNK cells by larger NGO-α-hCD16 with respect to smaller nanoclusters and individual antibody molecules.

NGO-Templated Nanoclustering of α-hCD16 Enhances Its Ability To Trigger NK Cell Degranulation. We next determined whether such NGO-nanoclustered ligands deliver enhanced stimulation to NK cells with respect to solubilized individual molecules. Unusually for NK cell receptors, ligation of CD16 leads to full functional activation without the need for ligation of costimulatory receptors or integrins.[31] This solo action underpins the potency of NK cells in killing antibody-opsonized target cells. It is known, however, that CD16 stimulation via soluble individual molecules is much less effective than using ligand molecules that are anchored to a solid substrate.

To assay for NK cell activation, we assessed the level of CD107a, also known as LAMP-1, found at the cell surface. CD107a is a component of the lipid membranes that encapsulate cytolytic compounds such as perforin in vesicles or lytic granules within the NK cell cytoplasm. When NK cell cytotoxicity is triggered, these granule membranes fuse with the outer cell membrane, releasing the cytolytic compounds by exocytosis into the vicinity of the target cell. This is known as degranulation and is the key event in NK cell cytotoxic activity. The quantity of CD107a on the NK cell surface thus serves as a proxy for this degranulation. Here, we measured this surface expression of CD107a on a cell-by-cell basis using flow cytometry after 6 h incubation with different stimulating reagents.

Initially, we compared the level of CD107a when pNK cells were stimulated using NGO-α-hCD16 nanoclusters and soluble antibody. These experiments were carried out using NGO-α-hCD16 nanoclusters ∼150 nm across and containing ∼120−140 α-hCD16 molecules each across six NK cell donors and two independently prepared batches of NGO-α-hCD16. As for the earlier binding experiments, we enabled direct comparison of soluble and NGO-clustered α-hCD16 antibody by using the same overall concentration of antibody in both cases.

Strikingly, NGO-α-hCD16 nanoclusters delivered a substantial enhancement in pNK cell activation with average CD107a levels approximately double those generated by soluble antibody alone (Figure 4a,b) ($p < 0.05$). An average of 10.3% of the cells expressed CD107a at the surface when activated via NGO-α-hCD16 nanoclusters as opposed to only 5.7% by soluble individual antibody molecules. Furthermore, an increase in CD107a when NGO-α-hCD16 was used with respect to the soluble antibody value was seen in five out of six donors (Figure 4c). This is despite the variation in overall CD107a expression levels that is a natural consequence of human donor variability.

To see if the enhanced activation would persist across different nanocluster sizes, we repeated this experiment using substantially smaller NGO-α-hCD16 nanoclusters with size $72 \pm {}^{19}_{11}$ and $112 \pm {}^{67}_{32}$ molecules per nanocluster. These enhanced activation of NK cells in three out of three donors studied with on average 9.0% of cells positive for CD107a as opposed to only 4.4% with soluble antibody stimulation (Figure 4a−c, $p < 0.05$). Although the degree to which activation was enhanced when these smaller nanoclusters were used was slightly less than for the larger ∼150 nm nanoclusters, the difference is not statistically significant. This absence of any substantial change when the NGO sheet size is varied by a factor of 2 is intriguing. Arguably, it hints at a threshold nanocluster size to trigger enhanced NK cell activation that is less than or equal to the size of the smaller clusters, with relatively little increase in effectiveness when molecules are clustered further beyond this threshold.

Finally it should be noted that the majority of cytotoxic activity in physiological NK cell populations is mediated by only a 10−20% subset of the population that degranulate.[32] Thus, the fact that 10−20% of cells show strong degranulation in response to NGO-α-hCD16 is sufficient to be of physiological importance.

Enhanced Cytokine (IFN-γ) Secretion by NGO-Templated Nanoclustering of α-hCD16. In addition to killing target cells directly, activated NK cells also secrete cytokines to impact other immune responses. In particular, activated NK cells are a predominant source of the cytokine IFN-γ, whose functions include enhancing the T cell and macrophage mediated inflammatory response. Cytokine secretion can be uncoupled from cytolytic degranulation, as evidenced by different subsets of NK cells being especially proficient in these different effector functions, and thus we set out to determine whether or not this immune cell effector function is also enhanced by NGO-templated nanoclustering of cell-stimulating molecules.

For cytokine secretion measurements, we once again stimulated pNK cells using NGO-α-hCD16 nanoclusters. Here, we measured the secretion of IFN-γ from pre-existing cell stores by supernatant ELISA following 6 h cell stimulation in the presence of monensin and brefeldin A.[33,34] Stimulation by individual α-hCD16 antibody molecules did not produce any increase in secreted IFN-γ with respect to unstimulated cells. In contrast, NGO-α-hCD16 stimulation increased IFN-γ secretion, an average 2.7-fold increase over background levels (Figure 4d) (average of three donors, $p < 0.05$). This directly demonstrates that NGO-templated nanoclustering of stimulating molecules enhances cytokine secretion via the CD16 receptor: a further indicator of the power of this technology, independent of the degranulation results above. To confirm that the increase in IFN-γ secretion was due to stimulation of the CD16 receptor and not the NGO construct itself, a control sample of NGO-α-mIgG1 was simultaneously tested and this did not trigger any IFN-γ secretion greater than nonstimulated cells.

In recent years, advances in microscopy and cell biology have increasingly revealed nanoscale molecular clusters as key signaling structures which impact immune cell function and development. Delivering clinical value from this insight is dependent on the creation of nanomaterials that can directly manipulate or interact with these nanostructures to a clinical purpose. The present study introduces NGO-templated molecular nanoclusters as a clear candidate, developing NGO-templated biomolecular nanostructures as biomimetic nanoclusters to trigger (or modulate) cellular activation. Notably, this has enabled the development of a new soluble reagent that activates of NK cells in isolation without requiring binding to a target surface. This opens up a significant new concept in the development of NK cell immunomodulatory

DOI: 10.1021/acs.nanolett.8b01089
Nano Lett. 2018, 18, 3282−3289

therapeutics, as well as a new application class for graphene-based bionanomaterials.

■ ASSOCIATED CONTENT

Supporting Information

The Supporting Information is available free of charge on the ACS Publications website at DOI: 10.1021/acs.nanolett.8b01089.

Methods; antibody-binding of NK cells at different concentrations; cell viability controls. (PDF)

■ AUTHOR INFORMATION

Corresponding Authors

*E-mail: i.dunlop@imperial.ac.uk.
*E-mail: daniel.davis@manchester.ac.uk.

ORCID

Daniel M. Davis: 0000-0002-9182-291X
Iain E. Dunlop: 0000-0002-6329-4996

Author Contributions

C.L. synthesized and characterized the nanomaterials and performed the NK cell experiments in collaboration with M.S. I.E.D. and D.M.D. conceived the project and supervised the research. I.E.D. and C.L. wrote the manuscript in collaboration with D.M.D.

Notes

The authors declare no competing financial interest.

■ ACKNOWLEDGMENTS

We acknowledge assistance from Kevin Stacey and Katja Srpan. The work was funded by EPSRC (EP/F500416/1) the Medical Research Council (Award G1001044), a Wellcome Trust Investigator Award (110091), and the Manchester Collaborative Centre for Inflammation Research (funded by a precompetitive open-innovation award from GSK, AstraZeneca, and The University of Manchester, United Kingdom).

■ REFERENCES

(1) Sharma, P.; Allison, J. P. The future of immune checkpoint therapy. *Science* **2015**, *348*, 56−61.
(2) Rosenberg, S. A.; Restifo, N. P. Adoptive cell transfer as personalized immunotherapy for human cancer. *Science* **2015**, *348*, 62−68.
(3) Liu, L.; Béziat, V.; Sheng, V. O. Y.; Pfefferle, A.; Schaffer, M.; Lehmann, S.; Hellström-Lindberg, E.; Söderhäll, S.; Heyman, M.; Grandér, D.; Malmberg, K.-J. Ex Vivo Expanded Adaptive NK Cells Effectively Kill Primary Acute Lymphoblastic Leukemia Cells. *Cancer Immunol. Res.* **2017**, *5*, 654.
(4) Rosenberg, S. A.; Yang, J. C.; Sherry, R. M.; Kammula, U. S.; Hughes, M. S.; Phan, G. Q.; Citrin, D. E.; Restifo, N. P.; Robbins, P. F.; Wunderlich, J. R.; Morton, K. E.; Laurencot, C. M.; Steinberg, S. M.; White, D. E.; Dudley, M. E. Durable complete responses in heavily pretreated patients with metastatic melanoma using T-cell transfer immunotherapy. *Clin. Cancer Res.* **2011**, *17*, 4550−4557.
(5) Qasim, W.; Brunetto, M.; Gehring, A. J.; Xue, S. A.; Schurich, A.; Khakpoor, A.; Zhan, H.; Ciccorossi, P.; Gilmour, K.; Cavallone, D.; Moriconi, F.; Farzhenah, F.; Mazzoni, A.; Chan, L.; Morris, E.; Thrasher, A.; Maini, M. K.; Bonino, F.; Stauss, H.; Bertoletti, A. Immunotherapy of HCC metastases with autologous T cell receptor redirected T cells, targeting HBsAg in a liver transplant patient. *J. Hepatol.* **2015**, *62*, 486−491.
(6) Fehniger, T. A.; Cooper, M. A. Harnessing NK Cell Memory for Cancer Immunotherapy. *Trends Immunol.* **2016**, *37*, 877−888.
(7) Guillerey, C.; Huntington, N. D.; Smyth, M. J. Targeting natural killer cells in cancer immunotherapy. *Nat. Immunol.* **2016**, *17*, 1025−1036.
(8) Dustin, M. L.; Chakraborty, A. K.; Shaw, A. S. Understanding the structure and function of the immunological synapse. *Cold Spring Harbor Perspect. Biol.* **2010**, *2*, a002311−a002311.
(9) Davis, D. M.; Dustin, M. L. What is the importance of the immunological synapse? *Trends Immunol.* **2004**, *25*, 323−327.
(10) Orange, J. S. Formation and function of the lytic NK-cell immunological synapse. *Nat. Rev. Immunol.* **2008**, *8*, 713−725.
(11) Dustin, M. L.; Depoil, D. New insights into the T cell synapse from single molecule techniques. *Nat. Rev. Immunol.* **2011**, *11*, 672−684.
(12) Lillemeier, B. F.; Mörtelmaier, M. A.; Forstner, M. B.; Huppa, J. B.; Groves, J. T.; Davis, M. M. TCR and Lat are expressed on separate protein islands on T cell membranes and concatenate during activation. *Nat. Immunol.* **2010**, *11*, 90−96.
(13) Oszmiana, A.; Williamson, D. J.; Cordoba, S. P.; Morgan, D. J.; Kennedy, P. R.; Stacey, K.; Davis, D. M. The Size of Activating and Inhibitory Killer Ig-like Receptor Nanoclusters Is Controlled by the Transmembrane Sequence and Affects Signaling. *Cell Rep.* **2016**, *15*, 1957−1972.
(14) Pageon, S. V.; Tabarin, T.; Yamamoto, Y.; Ma, Y.; Nicovich, P. R.; Bridgeman, J. S.; Cohnen, A.; Benzing, C.; Gao, Y.; Crowther, M. D.; Tungatt, K.; Dolton, G.; Sewell, A. K.; Price, D. A.; Acuto, O.; Parton, R. G.; Gooding, J. J.; Rossy, J.; Rossjohn, J.; Gaus, K. Functional role of T-cell receptor nanoclusters in signal initiation and antigen discrimination. *Proc. Natl. Acad. Sci. U. S. A.* **2016**, *113*, E6905−E6905.
(15) Pageon, S. V.; Cordoba, S. P.; Owen, D. M.; Rothery, S. M.; Oszmiana, A.; Davis, D. M. Superresolution Microscopy Reveals Nanometer-Scale Reorganization of Inhibitory Natural Killer Cell Receptors upon Activation of NKG2D. *Sci. Signaling* **2013**, *6*, ra62.
(16) Delcassian, D.; Depoil, D.; Rudnicka, D.; Liu, M.; Davis, D. M.; Dustin, M. L.; Dunlop, I. E. Nanoscale Ligand Spacing Influences Receptor Triggering in T Cells and NK Cells. *Nano Lett.* **2013**, *13*, 5608−5614.
(17) Matic, J.; Deeg, J.; Scheffold, A.; Goldstein, I.; Spatz, J. P. Fine Tuning and Efficient T Cell Activation with Stimulatory aCD3 Nanoarrays. *Nano Lett.* **2013**, *13*, 5090−5097.
(18) Cai, H.; Wolfenson, H.; Depoil, D.; Dustin, M. L.; Sheetz, M. P.; Wind, S. J. Molecular Occupancy of Nanodot Arrays. *ACS Nano* **2016**, *10*, 4173−4183.
(19) Singha, S.; Shao, K.; Yang, Y.; Clemente-Casares, X.; Solé, P.; Clemente, A.; Blanco, J.; Dai, Q.; Song, F.; Liu, S. W.; Yamanouchi, J.; Umeshappa, C. S.; Nanjundappa, R. H.; Detampel, P.; Amrein, M.; Fandos, C.; Tanguay, R.; Newbigging, S.; Serra, P.; Khadra, A.; Chan, W. C. W.; Santamaria, P. Peptide-MHC-based nanomedicines for autoimmunity function as T-cell receptor microclustering devices. *Nat. Nanotechnol.* **2017**, *12*, 701−710.
(20) Choudhuri, K.; Wiseman, D.; Brown, M. H.; Gould, K.; van der Merwe, P. A. T-cell receptor triggering is critically dependent on the dimensions of its peptide-MHC ligand. *Nature* **2005**, *436*, 578−582.
(21) Sun, X.; Liu, Z.; Welsher, K.; Robinson, J. T.; Goodwin, A.; Zaric, S.; Dai, H. Nano-graphene oxide for cellular imaging and drug delivery. *Nano Res.* **2008**, *1*, 203−212.
(22) Hong, H.; Yang, K.; Zhang, Y.; Engle, J. W.; Feng, L.; Yang, Y.; Nayak, T. R.; Goel, S.; Bean, J.; Theuer, C. P.; Barnhart, T. E.; Liu, Z.; Cai, W. In Vivo Targeting and Imaging of Tumor Vasculature with Radiolabeled, Antibody-Conjugated Nanographene. *ACS Nano* **2012**, *6*, 2361−2370.
(23) Zhang, L.; Lu, Z.; Zhao, Q.; Huang, J.; Shen, H.; Zhang, Z. Enhanced Chemotherapy Efficacy by Sequential Delivery of siRNA and Anticancer Drugs Using PEI-Grafted Graphene Oxide. *Small* **2011**, *7*, 460−464.
(24) Su, S.; Wang, J.; Vargas, E.; Wei, J.; Martínez-Zaguilán, R.; Sennoune, S. R.; Pantoya, M. L.; Wang, S.; Chaudhuri, J.; Qiu, J. Porphyrin Immobilized Nanographene Oxide for Enhanced and

DOI: 10.1021/acs.nanolett.8b01089
Nano Lett. 2018, 18, 3282−3289

Targeted Photothermal Therapy of Brain Cancer. *ACS Biomater. Sci. Eng.* **2016**, *2*, 1357−1366.
(25) Bunnell, S. C.; Hong, D. I.; Kardon, J. R.; Yamazaki, T.; McGlade, C. J.; Barr, V. A.; Samelson, L. E. T cell receptor ligation induces the formation of dynamically regulated signaling assemblies. *J. Cell Biol.* **2002**, *158*, 1263−1275.
(26) Gasparrini, F.; Feest, C.; Bruckbauer, A.; Mattila, P. K.; Müller, J.; Nitschke, L.; Bray, D.; Batista, F. D. Nanoscale organization and dynamics of the siglec CD22 cooperate with the cytoskeleton in restraining BCR signalling. *EMBO J.* **2016**, *35*, 258−280.
(27) Yang, K.; Wan, J.; Zhang, S.; Zhang, Y.; Lee, S. T.; Liu, Z. In Vivo Pharmacokinetics, Long-Term Biodistribution, and Toxicology of PEGylated Graphene in Mice. *ACS Nano* **2011**, *5*, 516−522.
(28) Ali-Boucetta, H.; Bitounis, D.; Raveendran-Nair, R.; Servant, A.; Van den Bossche, J.; Kostarelos, K. Purified Graphene Oxide Dispersions Lack In Vitro Cytotoxicity and In Vivo Pathogenicity. *Adv. Healthcare Mater.* **2013**, *2*, 433−441.
(29) Liu, Z.; Jiang, L.; Galli, F.; Nederlof, I.; Olsthoorn, R. C. L.; Lamers, G. E. M.; Oosterkamp, T. H.; Abrahams, J. P. A Graphene Oxidee-Streptavidin Complex for Biorecognition - Towards Affinity Purification. *Adv. Funct. Mater.* **2010**, *20*, 2857−2865.
(30) Venturelli, E.; Fabbro, C.; Chaloin, O.; Ménard-Moyon, C.; Smulski, C. R.; Da Ros, T.; Kostarelos, K.; Prato, M.; Bianco, A. Antibody Covalent Immobilization on Carbon Nanotubes and Assessment of Antigen Binding. *Small* **2011**, *7*, 2179−2187.
(31) Bryceson, Y. T.; March, M. E.; Ljunggren, H. G.; Long, E. O. Synergy among receptors on resting NK cells for the activation of natural cytotoxicity and cytokine secretion. *Blood* **2006**, *107*, 159−166.
(32) Vanherberghen, B.; Olofsson, P. E.; Forslund, E.; Sternberg-Simon, M.; Khorshidi, M. A.; Pacouret, S.; Guldevall, K.; Enqvist, M.; Malmberg, K. J.; Mehr, R.; Önfelt, B. Classification of human natural killer cells based on migration behavior and cytotoxic response. *Blood* **2013**, *121*, 1326−1334.
(33) Lamoreaux, L.; Roederer, M.; Koup, R. Intracellular cytokine optimization and standard operating procedure. *Nat. Protoc.* **2006**, *1*, 1507−1516.
(34) O'Neil-Andersen, N. J.; Lawrence, D. A. Differential modulation of surface and intracellular protein expression by T cells after stimulation in the presence of monensin or brefeldin A. *Clin. Diagn. Lab. Immunol.* **2002**, *9*, 243−250.

DOI: 10.1021/acs.nanolett.8b01089
Nano Lett. 2018, 18, 3282−3289